Modeling of a New Configuration for DFIGs Using T-type Converters and a Predictive Control Strategy in Wind Energy Conversion Systems

Rahim Ajabi-Farshbaf*‡, Mohammad Reza Azizian*, Sirvan Shazdeh*, Ataollah Mokhberdoran**

*Faculty of Electrical Engineering, Sahand University of Technology (SUT), Tabriz 51335-1996, Iran

**EFACEC Energia Máquinas e Equipamentos Eléctricos, S.A, Un. Switchgear & Automation, Rua Frederico Ulrich, PO Box 3078 4471-907, Maia, Portugal

(r_ajabi@sut.ac.ir, azizian@sut.ac.ir, s_shazdeh@sut.ac.ir, mokhber@fe.up.pt)

‡Corresponding Author; Rahim Ajabi-Farshbaf, Faculty of Electrical Engineering, Sahand University of Technology (SUT), Tabriz, Iran, Tel: +98 914 119 1050,

r_ajabi@sut.ac.ir

Received: 04.04.2016 Accepted:08.06.2016

Abstract- In this paper, a new topology is introduced for Doubly-Fed Induction Generators (DFIGs) applied in wind energy conversion systems. In the proposed topology T-type converters are used in back-to-back form instead of conventional converters. T-type converters are high-efficient three-level converters with high power quality. Furthermore, a hysteresis-based predictive control method is suggested for rotor current control of DFIG. Therefore, discrete models of the DFIG and T-type converters are extracted. A new equation is also defined for rotor current reference calculation which determines predictive current error. The suggested equation can be applied either for pre-connection to grid for synchronizing the DFIG or after connection to grid for regular control of DFIG. In addition to simulation results, the proposed topology is verified using a laboratory setup. The constructed setup is based on a 16-bit DSPIC and a wound-rotor induction machine. Simulation and practical results confirm effective operation of the proposed topology.

Keywords DFIGs; T-Type converters; hysteresis-based predictive control method; 16-bit DSPIC.

Nomenclature

General

R_s , R_r	Stator and rotor resistances
L_s ‘ L_r	Stator and rotor inductances
L_m	Magnetizing inductance
P	Pole pairs
J	Inertia momentum
V_{dc}	DC-link voltage
V_{c1}, V_{c2}	DC-link capacitors voltage
C	DC-link capacitors
F	Friction constant
T_{ij_g}	The j^{th} switch of the i^{th} phase of the grid-side converter
T_{ij_r}	The j^{th} switch of the i^{th} phase of the rotor-side converter
t_s	Sampling time
ω_s	Synchronous speed

Superscripts

k	The calculated values at k^{th} sampling time
k + y	The predicted values at $(k+y)^{th}$ sampling time
*	Vector conjugate
Ref	Reference values

Subscripts

ds , qs	Stator dq reference frames
dr , qr	Rotor dq reference frames

1. Introduction

Increased penetration of wind energy conversion systems in distribution networks requires new functional strategies to improve the efficiency and power quality. DFIG is one of the most common and economical topologies, which is used in wind energy conversion systems with many practical usages. DFIG consists of a wound rotor induction machine, which its rotor windings are connected to the grid using a back-to-back converter and a transformer. Rotor-side converter controls rotor speed to obtain optimized operating point in every wind speed. On the other hand, grid-side converter adjusts DC link voltage. Nominal power capacity of the DFIG converters is a fraction of machine nominal capacity, which is the main characteristic of DFIGs [1].

DC/AC converters, which are used in variable speed wind turbines, create harmonic contents. Therefore, harmonic filters are proposed to solve switching harmonics in practical applications. However, since these filters are composed of capacitors and inductances, LC oscillations may be created. Another solution to decrease the harmonic content is to increase switching frequency; in this condition, one of the main problems is dV/dt on switches [2]. Applying multi-level inverters is another solution to decrease the harmonic content. In the same working condition, it is possible that switching frequency of multi-level converters to be 25% less than switching frequency of two-level converters; while, harmonic content would be the same. Different references have presented many multi-level structures for using in DFIG [3]. In [3] and [4], a review is presented on power converters and their advantages especially multi-level converters, which are used in wind energy conversion systems. In [5], a nine-switch converter is suggested for DFIGs. In [6], matrix converter is applied for connection of DFIG to grid. Design procedure of three-level Neutral-Point-Clamped (NPC) converter parameters is extensively presented in [7]. In [8], three-level T-type converter is used for solar power generation systems.

T-Type converters are three-level converters with high efficiency. This converter circuit and its performance details are presented in [9]. Nowadays, three-level converters, in case of standard implementation, have high power transmission capability and need smaller filters. Further, the ability to perform in high voltage levels results in gaining greater attention comparing two-level converters. In addition, T-type three-level converters have more advantages than two-level converters and at the same operating conditions including, low conduction losses, low electric stresses on switches, low switching frequency, low output voltage harmonics and low current harmonics, as well as high voltage quality [10, 11]. T-type converter can be controlled and switched by using conventional switching methods such as PWM and SVPWM. Fig.1 illustrates the research proposed structure.

Also, a strategy is presented for rotor current control which relies on predictive control approach extracted from the DFIG discrete model. Recently, predictive controlling approaches gained lots of attention due to simple implementation and achieving better results [12, 13]. These algorithms are used in different applications and references because of their performance and straight-forwardness [14, 15]. In [16], predictive control fundamentals are presented. Moreover, several predictive control algorithms, such as deadbeat control, hysteresis based control, trajectory based control, Model Predictive Control (MPC) are reviewed and presented in [17] for controlling of power converters and drives. In [18] and [19], a predictive control strategy is developed for DFIG systems equipped with multilevel and matrix converters, respectively.

This paper presents a new topology for DFIGs which is based on T-type converters. Although, T-type converters are used in previous works such as [8-10], it is the first time that the T-type converters are used in the DFIG structure. This research tries to obtain a novel industrial application for T-type converter, which seems to be more useful converter compared with similar converters, in DFIG wind energy conversion systems with a relatively simple predictive control algorithm. Simple implementation and control of the proposed topology, is its main advantage which is an important issue in industry applications. Another main advantage of the T-type converters is their low loss which is extensively discussed in [9]. Moreover, a current control strategy for rotor circuit is extracted and formulated based on predictive control strategies. The predictive control approach, in this research, determines the optimized switching pattern for rotor-side T-type converter. In this way, the rotor current traces down the reference current. To control the converter, hysteresis current controller is used. The hysteresis based predictive control algorithm needs no modulator and is based on simple concepts [16-17]. The results are simulated by MATLAB/Simulink indicating proper performance of the proposed structure and the designed control approach. The paper presents some experimental tests on a prototype setup realized in the laboratory which proves the simple control of the proposed topology and confirms the proposed structure. The controlling system, used in laboratory setup, is implemented by a DSPIC processor.

The paper is organized as follows. The second section presents DFIG dynamic model. In Section 3, T-type converter is modelled. Modelling constraints are applicable in this article and more details are presented in [9]. In Section 4, the presented model in second section is discretised, the proposed approach is formulated and the converter switching approach is also subjected; Section 5 includes simulation results and in Section 6, laboratory results are explained; finally, the conclusion part is in Section 7.

2. DFIG Dynamic Model

In this section, DFIG dynamic model is briefly presented in synchronous rotating reference frame. Eq. (1) introduces stator and rotor electric variables of DFIG dynamic model in synchronous reference frame in matrix form [1]:

$$\begin{bmatrix} v_{ds} \\ v_{qs} \\ v_{dr} \\ v_{qr} \end{bmatrix} = \begin{bmatrix} R_s+L_sD & -\omega_s L_s & L_mD & -\omega_s L_m \\ \omega_s L_s & R_s+L_sD & \omega_s L_m & L_mD \\ L_mD & -\omega_r L_m & R_r+L_rD & -\omega_r L_r \\ \omega_r L_m & L_mD & \omega_r L_r & R_r+L_rD \end{bmatrix} \begin{bmatrix} i_{ds} \\ i_{qs} \\ i_{dr} \\ i_{qr} \end{bmatrix} \quad (1)$$

State equations with current variables are also obtained as Eq. (2) by algebraically rewriting Eq. (1) where, D is differential operator $(D = \frac{d}{dt})$ and $\omega_r = \omega_s - \omega_m$.

DFIG electromagnetic torque equation is shown by Eq. (3). Rotor electric angular speed ω_m is extracted from Eq. (3) according to Eq. (4).

$$T_e = \frac{3}{2} P\, \mathrm{Im}\{\overrightarrow{\Psi_s}.\overrightarrow{I_r^*}\} = \frac{3}{2} L_m P\, \mathrm{Im}\{\overrightarrow{I_s}.\overrightarrow{I_r^*}\}$$
$$= \frac{3}{2} L_m P(i_{qs} i_{dr} - i_{ds} i_{qr}) = \frac{J}{P}\frac{d\omega_m}{dt} + \frac{F}{P}\omega_m + T_T \quad (3)$$

$$\frac{d\omega_m}{dt} = \frac{P}{J}\left(\frac{3}{2} L_m P(i_{qs} i_{dr} - i_{ds} i_{qr}) - \frac{F}{P}\omega_m - T_T\right) \quad (4)$$

More details are discussed in [1].

$$D\begin{bmatrix} i_{ds} \\ i_{qs} \\ i_{dr} \\ i_{qr} \end{bmatrix} = \left(\frac{1}{L_s L_r - L_m^2}\right)\left(\begin{bmatrix} -R_s L_r & \omega_s L_s L_r - \omega_r L_m^2 & L_m R_r & (\omega_s L_r L_s - \omega_r L_s L_m) \\ -(\omega_s L_r L_s - \omega_r L_m^2) & -R_s L_r & -(\omega_s - \omega_r) L_m L_r & L_m R_r \\ L_m R_s & -(\omega_s - \omega_r) L_m L_s & -L_s R_r & -(\omega_s L_m^2 - \omega_r L_s^2) \\ (\omega_s - \omega_r) L_m L_s & L_m R_s & \omega_s L_m^2 - \omega_r L_s L_r & -L_s R_r \end{bmatrix}\begin{bmatrix} i_{ds} \\ i_{qs} \\ i_{dr} \\ i_{qr} \end{bmatrix} + \right.$$
$$\left.\begin{bmatrix} L_r & 0 & -L_m & 0 \\ 0 & L_r & 0 & -L_m \\ -L_m & 0 & L_s & 0 \\ 0 & -L_m & 0 & L_s \end{bmatrix}\begin{bmatrix} v_{ds} \\ v_{qs} \\ v_{dr} \\ v_{qr} \end{bmatrix}\right) \quad (2)$$

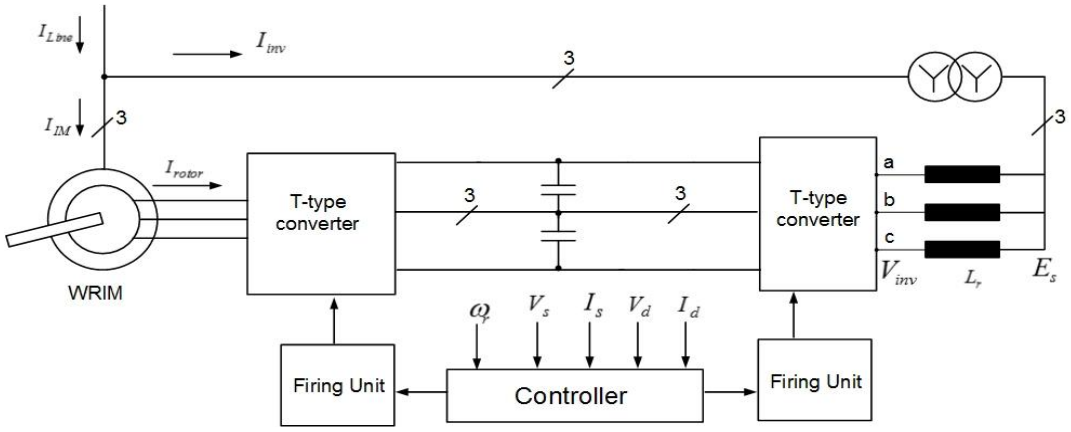

Fig. 1. Proposed structure for DFIG with T-type converter in back-to-back form.

3. T-Type Converter Modeling

In this section, T-type converter model is provided, which is used in back-to-back form in the proposed structure. Fig.2 illustrates the T-type converter circuit structure.

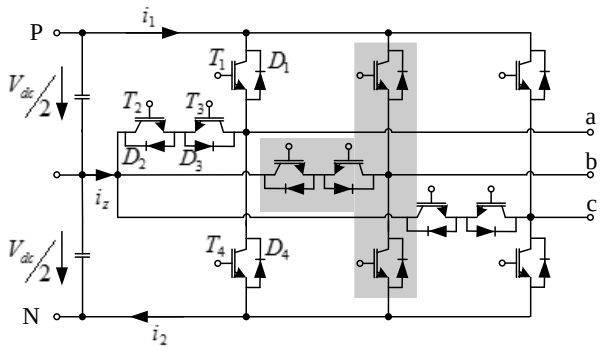

Fig. 2. T-type converter circuit.

Table 1. also shows different switching modes in order to reach the desired output voltage. According to this

switching pattern current naturally and independent from its direction shifts correctly between switching branches.

Table 1. T-type converter switching modes [9]

Mode	V_{out}	T_1	T_2	T_3	T_4
Positive	$+\frac{V_{dc}}{2}$	1	1	0	0
Neutral	0	0	1	1	0
Negative	$-\frac{V_{dc}}{2}$	0	0	1	1

Now, converter output AC voltages are extracted in matrix form according to table (1) and presented more details in [9, 20]:

$$\begin{bmatrix} V_{an} \\ V_{bn} \\ V_{cn} \end{bmatrix} = \frac{V_{c1}}{3}\begin{bmatrix} 2 & -1 & -1 \\ -1 & 2 & -1 \\ -1 & -1 & 2 \end{bmatrix}\begin{bmatrix} T_{a1} \\ T_{b1} \\ T_{c1} \end{bmatrix} + \frac{V_{c2}}{3}\begin{bmatrix} 2 & -1 & -1 \\ -1 & 2 & -1 \\ -1 & -1 & 2 \end{bmatrix}\begin{bmatrix} T_{a2} \\ T_{b2} \\ T_{c2} \end{bmatrix} \quad (5)$$

It should be notified that capacitors voltages are not exactly equal. Current flow from grid side converter is modelled as follow:

$$\begin{bmatrix} i_{1\_g} \\ i_{2\_g} \end{bmatrix} = \begin{bmatrix} T_{a1\_g} & T_{b1\_g} & T_{c1\_g} \\ T_{a2\_g} & T_{b2\_g} & T_{c2\_g} \end{bmatrix}\begin{bmatrix} i_{a\_g} \\ i_{b\_g} \\ i_{c\_g} \end{bmatrix} \quad (6)$$

In Eq. (6), subscript 'g' refers to grid-side converter parameters; rotor-side converter model is also as follows:

$$\begin{bmatrix} i_{1\_r} \\ i_{2\_r} \end{bmatrix} = \begin{bmatrix} -T_{a1\_r} & -T_{b1\_r} & -T_{c1\_r} \\ -T_{a2\_r} & -T_{b2\_r} & -T_{c2\_r} \end{bmatrix}\begin{bmatrix} i_{a\_r} \\ i_{b\_r} \\ i_{c\_r} \end{bmatrix} \quad (7)$$

In Eq. (7), subscript 'r' represents rotor-side converter. DC link modelling requires calculating DC bus voltage, which must be based on current passing from capacitors.

$$V_C = \frac{1}{C}\int i_C dt \quad (8)$$

According to DC currents directions in rotor-side and grid-side converters, passing current for each of the DC link capacitors can be calculated as follows:

$$\begin{bmatrix} i_{c1} \\ i_{c2} \end{bmatrix} = \begin{bmatrix} 1 & -1 & 0 & 0 \\ -1 & -1 & -1 & -1 \end{bmatrix}\begin{bmatrix} i_{1\_r} \\ i_{1\_g} \\ i_{z\_r} \\ i_{z\_g} \end{bmatrix} \quad (9)$$

where, according to Fig.2 i_{z_r}, i_{z_g}, i_{1_r}, i_{1_g} are current flow from DC link to rotor- and grid-side converters and from neutral point to rotor- and grid-side converters, respectively. Finally, the DC link of the T-type converter can be modelled as flow:

$$\begin{bmatrix} i_{c1} \\ i_{c2} \end{bmatrix} = \begin{bmatrix} -T_{a1\_r} & -T_{b1\_r} & -T_{c1\_r} \\ -T_{a2\_r} & -T_{b2\_r} & -T_{c2\_r} \end{bmatrix}\begin{bmatrix} i_{a\_r} \\ i_{b\_r} \\ i_{c\_r} \end{bmatrix} + \begin{bmatrix} T_{a1\_g} & T_{b1\_g} & T_{c1\_g} \\ -T_{a2\_g} & -T_{b2\_g} & -T_{c2\_g} \end{bmatrix}\begin{bmatrix} i_{a\_g} \\ i_{b\_g} \\ i_{c\_g} \end{bmatrix} \quad (10)$$

The converter requires zero average neutral-point current for stable neutral-point voltage. The small dc-link capacitors may not maintain capacitor voltage balance, even with zero neutral-point current. This may happen due to nonlinearities present in the circuit. This requires a fast control of the neutral-point voltage.

4. Proposed Control Approach

Figure 3 represents proposed control method. This control approach is implemented in dq synchronous reference frame. In the studied model in previous sections; a set of variables exist, which their value differ in time domain, even in steady state. Since two back-to-back converters exist, multiple switching modes may be applied on the system, the best of which with least error of reference and predicted amount will be applied to the system. In the aforementioned approach, the machine mechanical speed ω_m, and its angle θ_m are calculated by an encoder and grid electric angular speed ω_g and its angle θ_g are a PLL output which is synchronous with grid. To select the best switching mode in the sampling time t_s^{k+1}, i.e. s_i^{k+1}, stator voltage V_s^{k+1} and rotor current i_r^{k+2} must be predicted in order to trace the rotor reference current i_r^{ref} down. This approach relies on Euler derivation equation (11) offered as numerical approximation resulted in Eq. (12).

$$f'(\chi) = \frac{f(\chi_0 + h) - f(\chi_0)}{h} \quad (11)$$

Eq. (12) is subjected to the discrete derivative to predict the essential amount of the next sampling period.

$$\frac{\Delta f(\chi)}{\Delta t} \approx \frac{f(k+1) - f(k)}{t_s} \quad (12)$$

Using Eq. (12) differential equations (2) and (4) can be calculated.

4.1. Discretising Equations of DFIG Model

Considering proposed control algorithm and using Eq. (2), Eq. (6) and Eq. (11), the predicted rotor currents and rotor angular speed amount obtained by Eq. (13), which is shown on the top of next page. We also have:

$$\omega_r^k = \omega_s - \omega_m^k \tag{14}$$

$$\omega_m^{k+1} = \frac{P}{J}\left(\frac{3}{2} L_m P(i_{qs}^k i_{dr}^k - i_{ds}^k i_{qr}^k) - \frac{F}{P}\omega_m^k - T_T^k\right) t_s + \omega_m^k \tag{15}$$

In Eq. (13), constants λ_1 to λ_{18} are obtained by simplification of Eq. (2), shown in appendix 1. Since before connecting to grid we have i_s=0, in order to synchronization, the related statements to DFIG rotor currents and angular speed are simplified as Eq. (16) and Eq. (17), respectively.

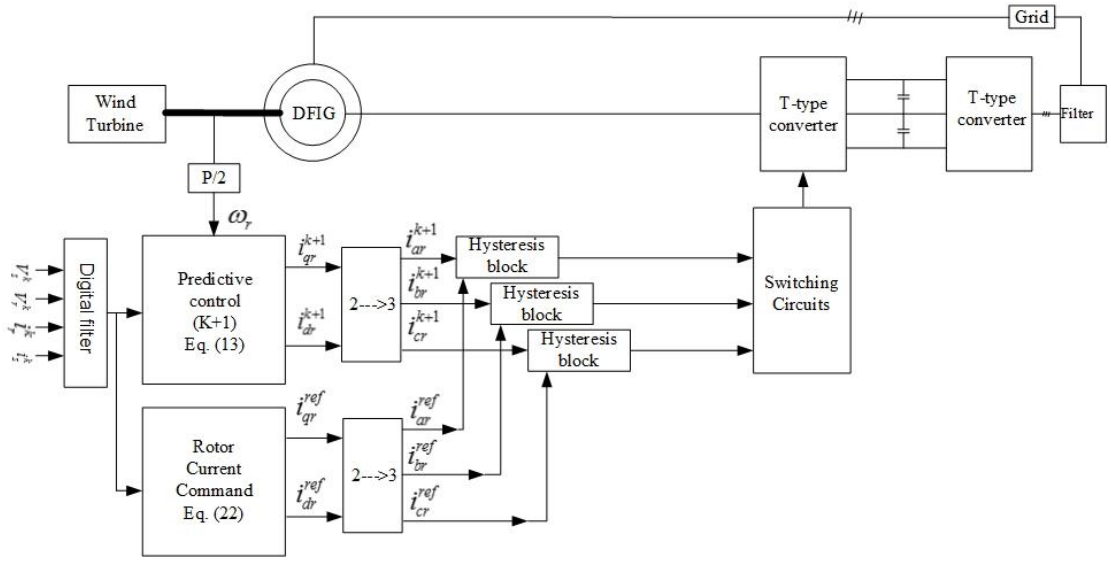

Fig. 3. Proposed hysteresis-based control algorithm for controlling of rotor current in the rotor side T-type converter.

$$\begin{bmatrix} i_{ds}^{k+1} \\ i_{qs}^{k+1} \\ i_{dr}^{k+1} \\ i_{qr}^{k+1} \end{bmatrix} = \lambda_1 \left(\begin{bmatrix} -\lambda_5 & (\lambda_6 - \lambda_7\omega_r^k) & \lambda_9 & (\lambda_{10} - \lambda_{11}\omega_r^k) \\ -(\lambda_6 - \lambda_7\omega_r^k) & -\lambda_{12} & -(\lambda_{10} - \lambda_{13}\omega_r^k) & \lambda_9 \\ \lambda_{14} & -(\lambda_{15} - \lambda_{11}\omega_r^k) & -\lambda_{16} & -(\lambda_{17} - \lambda_8\omega_r^k) \\ (\lambda_{15} - \lambda_{11}\omega_r^k) & \lambda_{14} & (\lambda_{17} - \lambda_{18}\omega_r^k) & -\lambda_{16} \end{bmatrix} \begin{bmatrix} i_{ds}^k \\ i_{qs}^k \\ i_{dr}^k \\ i_{qr}^k \end{bmatrix} t_s + \begin{bmatrix} \lambda_2 & 0 & \lambda_3 & 0 \\ 0 & \lambda_2 & 0 & \lambda_3 \\ \lambda_3 & 0 & \lambda_4 & 0 \\ 0 & \lambda_3 & 0 & \lambda_4 \end{bmatrix} \begin{bmatrix} v_{ds}^k \\ v_{qs}^k \\ v_{dr}^k \\ v_{qr}^k \end{bmatrix} t_s \right) + \begin{bmatrix} i_{ds}^k \\ i_{qs}^k \\ i_{dr}^k \\ i_{qr}^k \end{bmatrix} \tag{13}$$

$$\frac{1}{t_s}\begin{bmatrix} i_{ds}^{k+1} - i_{ds}^k \\ i_{qs}^{k+1} - i_{qs}^k \end{bmatrix} = \lambda_1 \begin{bmatrix} -\lambda_5 & (\lambda_6 - \lambda_7\omega_r^{ref}) & \lambda_9 & (\lambda_{10} - \lambda_{11}\omega_r^{ref}) \\ -(\lambda_6 - \lambda_7\omega_r^{ref}) & -\lambda_{12} & -(\lambda_{10} - \lambda_{13}\omega_r^{ref}) & \lambda_9 \end{bmatrix} \begin{bmatrix} i_{ds}^k \\ i_{qs}^k \\ i_{dr}^k \\ i_{qr}^k \end{bmatrix} + \begin{bmatrix} \lambda_2 & \lambda_3 & 0 \\ 0 & 0 & \lambda_3 \end{bmatrix} \begin{bmatrix} V_s \\ v_{dr}^k \\ v_{qr}^k \end{bmatrix} \tag{21}$$

$$\begin{bmatrix} i_{dr}^{k+1} \\ i_{qr}^{k+1} \end{bmatrix} = \lambda_1 \left(\begin{bmatrix} -\lambda_{16} & -(\lambda_{17} - \lambda_8\omega_r^k) \\ (\lambda_{17} - \lambda_{18}\omega_r^k) & -\lambda_{16} \end{bmatrix} \begin{bmatrix} i_{dr}^k \\ i_{qr}^k \end{bmatrix} t_s + \begin{bmatrix} \lambda_3 & 0 & \lambda_4 & 0 \\ 0 & \lambda_3 & 0 & \lambda_4 \end{bmatrix} \begin{bmatrix} v_{ds}^k \\ v_{qs}^k \\ v_{qr}^k \\ v_{qr}^k \end{bmatrix} t_s \right) + \begin{bmatrix} i_{dr}^k \\ i_{qr}^k \end{bmatrix} \tag{16}$$

$$\omega_m^{k+1} = \frac{P}{J}\left(-\frac{F}{P}\omega_m^k - T_T^k\right) t_s + \omega_m^k \tag{17}$$

Furthermore, stator voltage, considering stator current equal with zero, can be calculated by solving (13) as follows:

$$V_{ds}^k = -\frac{\lambda_3 v_{dr}^k + \lambda_9 i_{dr}^k + (\lambda_{10} - \lambda_{11}\omega_r^k) i_{qr}^k}{\lambda_2} \tag{18}$$

$$V_{qs}^k = -\frac{\lambda_3 v_{qr}^k - (\lambda_{10} - \lambda_{13}\omega_r^k) i_{qr}^k + \lambda_9 i_{dr}^k}{\lambda_2} \tag{19}$$

4.2. Calculation of Rotor Current Command

For determination of rotor current reference value, the stator voltage equation in vector form is used. In synchronous reference frame, we have,

$$V_{sdq} = R_s i_{sdq}^k + L_s\left(\frac{i_s^{k+1} - i_s^k}{t_s}\right) + L_m\left(\frac{i_r^{k+1} - i_r^k}{t_s}\right) + j\omega_s L_s i_s^k + j\omega_s L_m i_r^k \quad (20)$$

where considering Eq. (22) on the top of this page and by simplification of (20) and (21), rotor current reference value is as follows:

$$i_{rdq}^{ref} = \left(V_s - R_s i_{sdq}^k - L_s\left(\frac{i_{sdq}^{k+1} - i_{sdq}^k}{t_s}\right) - j\omega_s L_s i_{sdq}^k - j\omega_s L_m i_{rdq}^k\right)\frac{t_s}{L_m} + i_{rdq}^k \quad (22)$$

where, $\omega_r = \omega_s - \omega_m$, $\omega_r^{ref} = \omega_s - \omega_m^{ref}$.

4.3. Selection of Switching Pattern

According to discretised system model, applied control algorithm will be simple and straightforward. The purpose of this approach is to select the next optimized switching pattern, s_i^{k+1}, for converter; the controller is essential to provide the suitable rotor voltage space vector, V_r, and the least possible error between predicted and reference rotor current. For this purpose the predicted rotor current from Eq. (13) is compared with reference rotor current, which is calculated from Eq. (22), using a hysteresis block. Both predicted and reference rotor currents are transformed to abc-frame and then passes from hysteresis blocks. Hysteresis controller is set with a limited bandwidth to control rotor current in desired values. The suggested method is in fact a current regulator. Therefore, in order to predict stator and rotor currents and voltages in the Sample k+1, it is necessary to measure their real values in the Sample k. Then, predicted rotor currents are compared with command values. For tracking of command value by measured value a hysteresis block is considered for minimizing established error. Figure 3 illustrates the switching pattern of the proposed predictive algorithm.

5. Simulation Results

In this section, simulation results are presented using MATLAB/Simulink in order to validate the controlling approach of the proposed topology of DFIG based on T-type converters. Simulation conducted in two parts. In first part, wind speed steps down in Second 5; and in second part, wind speed steps up at the same time and the dynamic response of the induction machine parameters will be verified. Fig.4 to 6 illustrate simulation results in exchange for wind speed decrease. Figure 4 represents changing in wind speed and induction machine rotor speed. Wind speed decreases from 15m/s to 10m/s, which naturally leads to rotor speed reduction. Figure 5 shows DC link voltage and reactive and active powers. The proposed topology in this figure efficiently stabilizes DC link voltage. Figure 6 evaluates converter performance. The changes in rotor currents and voltages of the grid-side and rotor-side converters are represented in this figure. Grid-side and rotor-side converters are switching by PWM method and proposed hysteresis-based predictive control strategy, respectively. These figures confirm the research proposed structure performance, especially in rotor current control.

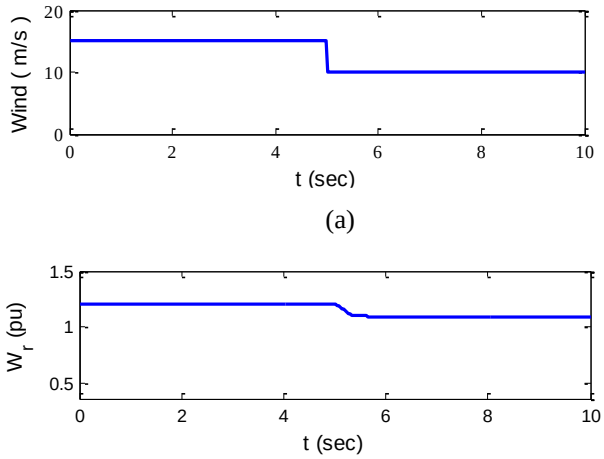

Fig. 4. a) Wind speed b) Rotor speed with decreasing wind speed from 15 to 10 m/s.

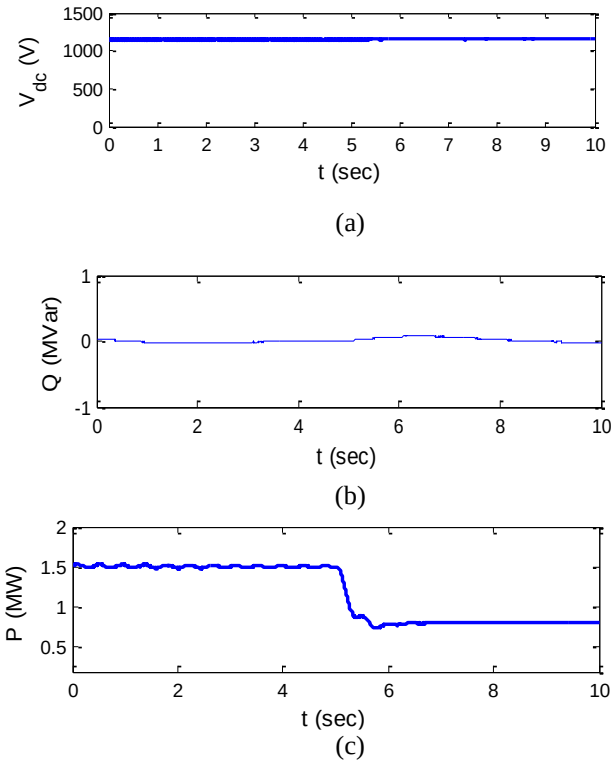

Fig. 5. a) DC link voltage b) Reactive power c) Active power changes with decreasing wind speed from 15 to 10 m/s.

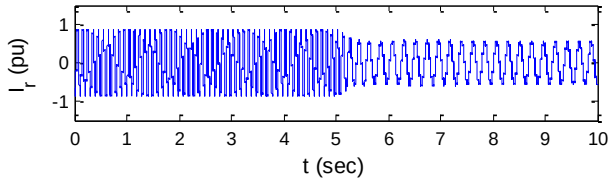

(a)

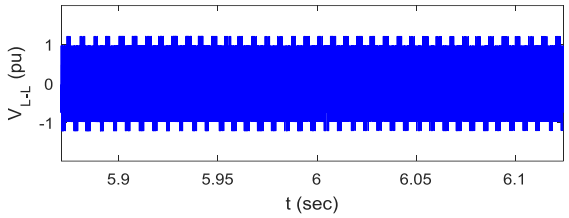

(b)

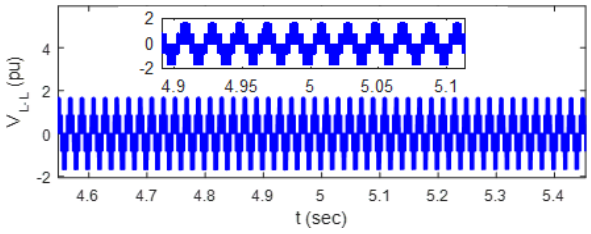

(c)

Fig. 6. a) Rotor current b) Rotor-side converter voltage c) Grid-side converter voltage with decreasing wind speed wind speed from 15 to 10 m/s.

Similar results are extracted in increasing wind speed exchange, shown in Fig.7 to 9. In Fig.7, wind speed and induction machine rotor speed changes are presented. Wind speed increases from 10 to 15 m/s, which leads to increased rotor speed. Fig.8 represents DC link voltage and reactive and active powers. In these conditions performance of the proposed topology are appropriate to stabilize DC-link voltage. In Fig.9, converters performances are evaluated. Changes in rotor current, grid-side converter and rotor-side converters voltages are presented in this figure indicating effective operation of the suggested model.

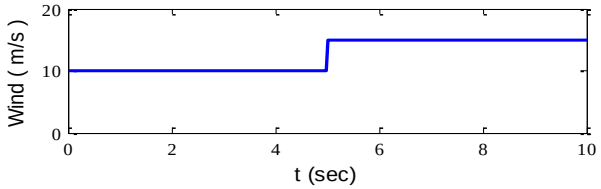

(a)

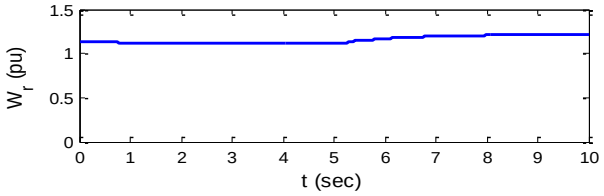

(b)

Fig. 7. a) Wind speed b) Rotor speed with increasing wind speed from 10 to 15 m/s.

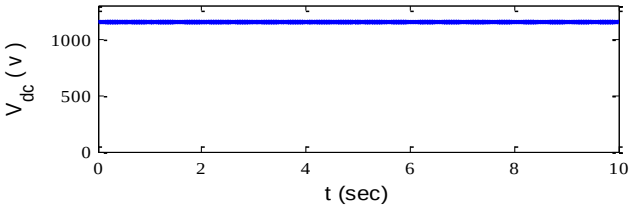

(a)

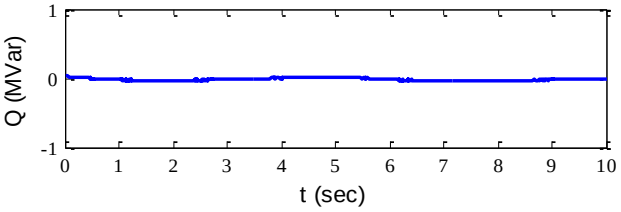

(b)

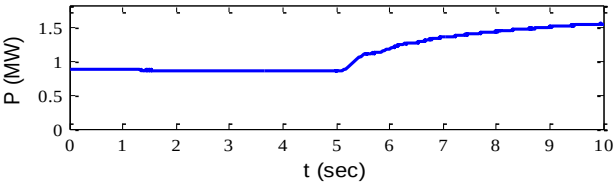

(c)

Fig. 8. a) DC link voltage b) Reactive power c) Active power changes with increasing wind speed from 10 to 15 m/s.

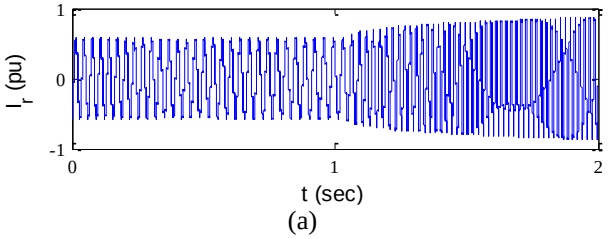

(a)

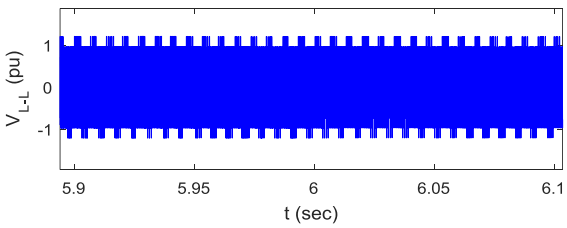

(b)

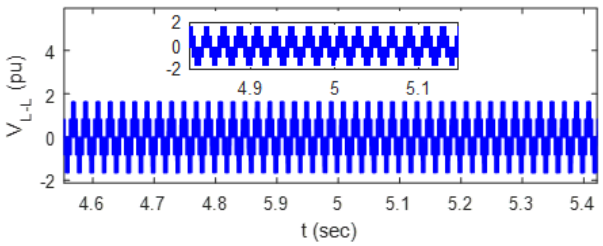

(c)

Fig. 9. a) Rotor current b) Rotor-side converter voltage c) Grid-side converter voltage with increasing wind speed from 10 to 15 m/s.

The transient response of the proposed method is strongly depends on the machine inertia momentum (J). Since the J is big in the simulated machine, machine response to the speed changes is slow and therefore rotor current changes smoothly, which is represented in Fig.6a and 9a.

Proposed controller precision is proved in Fig.10 and 11 for wind speed decrease and increase, respectively. In these figure rotor current reference and measured values are represented in dq reference frame. As it can be seen the established error in both case studies is less than 0.01 p.u. and acceptable.

Finally, harmonic content of a T-type converter is compared with a NPC converter. As it mentioned previously, harmonic content of T-type converter in similar conditions is more desirable than other converters, which is depicted in Fig.12. THD of T-type converter is relatively less than THD of NPC converter.

6. Practical Results

Some dynamic behaviours of the proposed structure is evaluated by a laboratory setup. The experimental system is consisted of (1) a DC motor considered as rotor actuator and counted as wind turbine; (2) an induction machine, which in use machine related parameters are in appendix 2; and (3) in order to create switching pulses to drive IGBTs, a 16-bit digital signal controller, dspIC30F4011 is used as controller [21]. Any T-type converter requires 12 IGBTs, in which each IGBT must be driven by the mentioned controller. Fig.13 presents the applied laboratory setup

Fig.14a depicts voltage of grid-side T-type converter and Fig.14b illustrates rotor current in the steady-state with rotor speed. In Fig.14a, the three-level shape is determined. In the constructed laboratory setup, snubber circuit isn't used. Therefore, because of inductances of the setup especially stray inductances of the IGBTs, L.di/dt leads to the voltage jumps in the switching instants. Since the used scope has high sampling rate (1 Giga Sample per Second), the voltage jumps have appeared in the Fig. 14a.

Practical results also represent appropriate performance of DFIG by using back-to-back T-type converters. Rotor-side T-type converter dynamic performance is presented in two modes: in first mode DC motor speed increases and in second mode DC motor speed decreases, the results of changing in rotor current are shown in Fig.15 for one phase, indicating that current changes represent desired operation of proposed structure.

Since the moment of inertia (J) is small in the laboratory setup, machine response to the speed changes is fast and therefore rotor current settles rapidly in new operating point and steady state, which is depicted in Fig.15.

Since practical systems are usually based on discrete sampling and predictive control algorithms are also based on discrete modelling of the plant, implementation of the proposed method is relatively simple. On the other hand, compared with conventional PI controllers, where correct tuning of its coefficients needs more analysis, predictive controllers are superior.

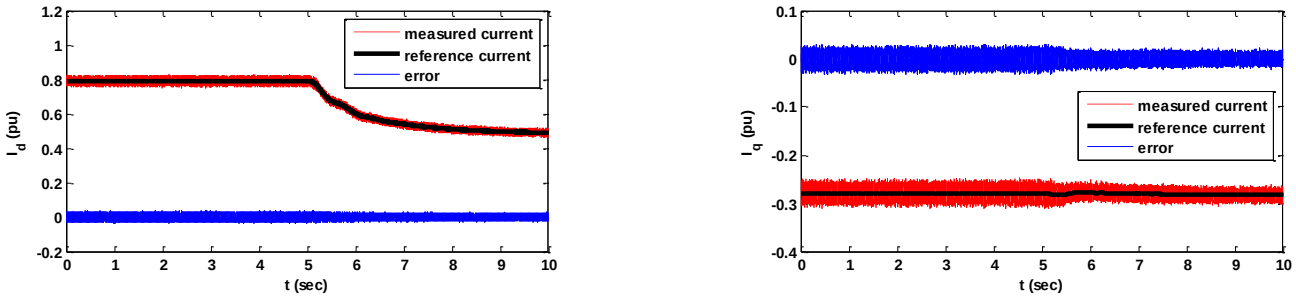

(a) (b)

Fig. 10. Rotor current tracking error with increasing wind speed from 10 to 15 m/s a) d-axes current b) q-axes current.

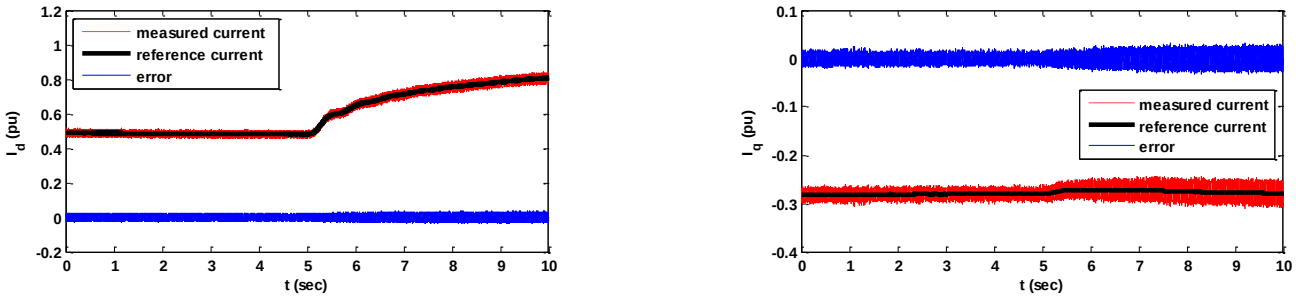

(a) (b)

Fig. 11. Rotor current tracking error with increasing wind speed from 10 to 15 m/s a) d-axes current b) q-axes current.

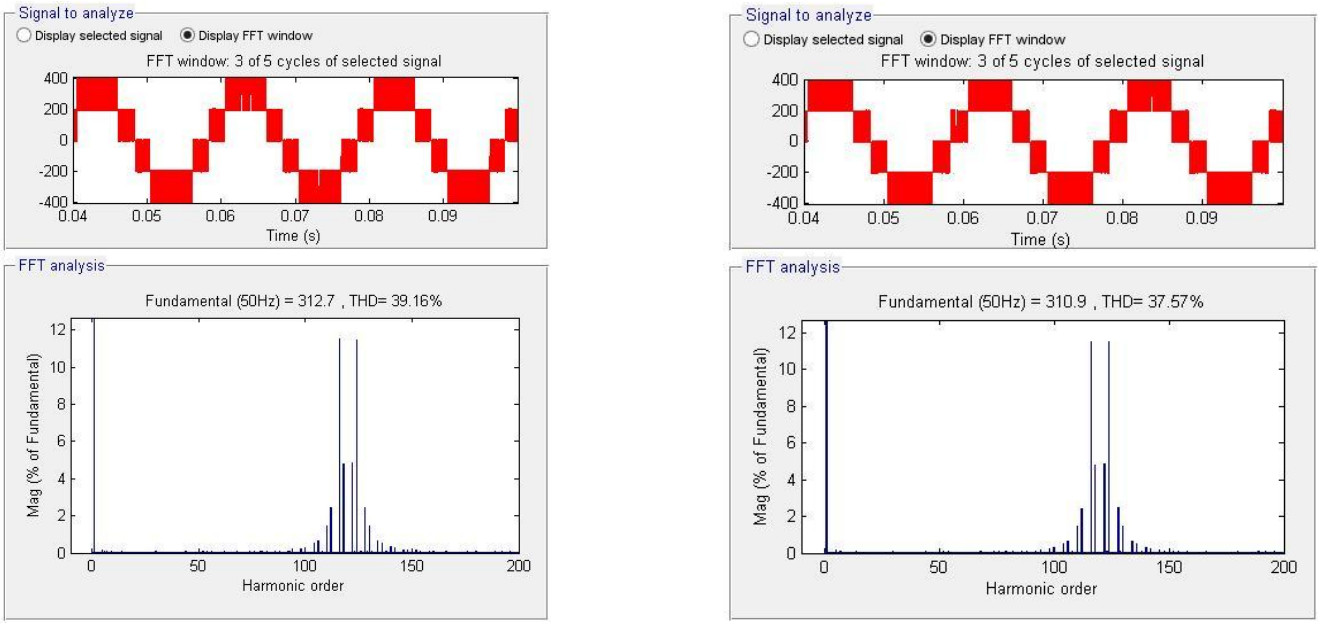

(a) (b)

Fig. 12. THD of a) NPC converter (39.16%) b) T-type converter (37.57%).

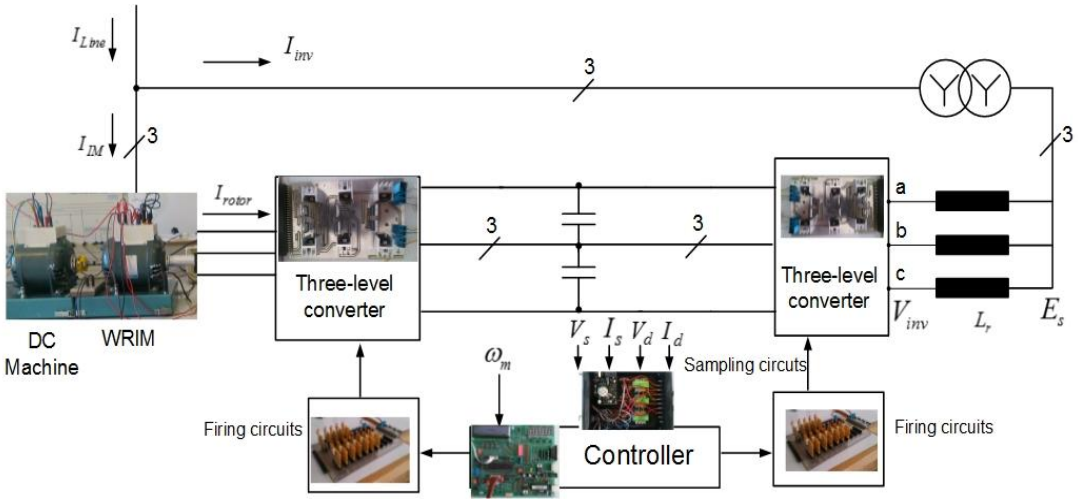

Fig. 13. Applied laboratory setup.

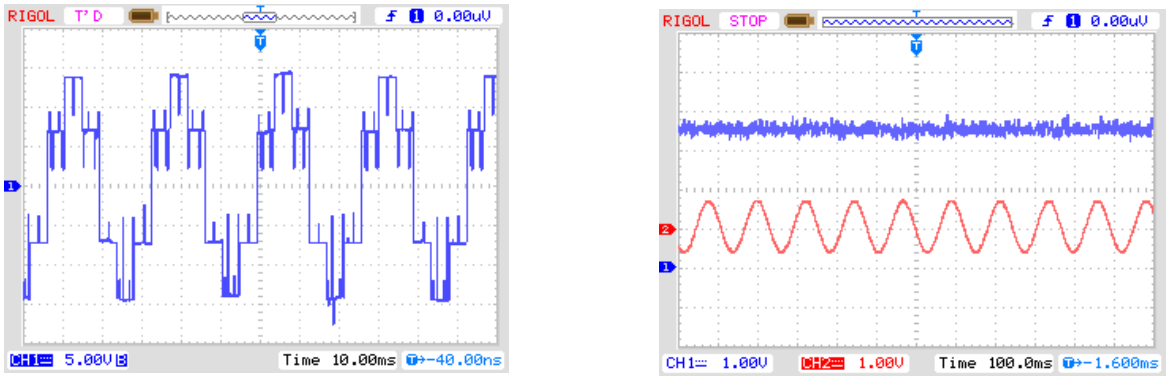

(a) (b)

Fig. 14. a) Waveform of the grid-side T-Type converter voltage, b) Waveform of rotor current and rotor speed in steady state (Fig.14b; CH1: 1A/div and CH2: 1000rpm/div).

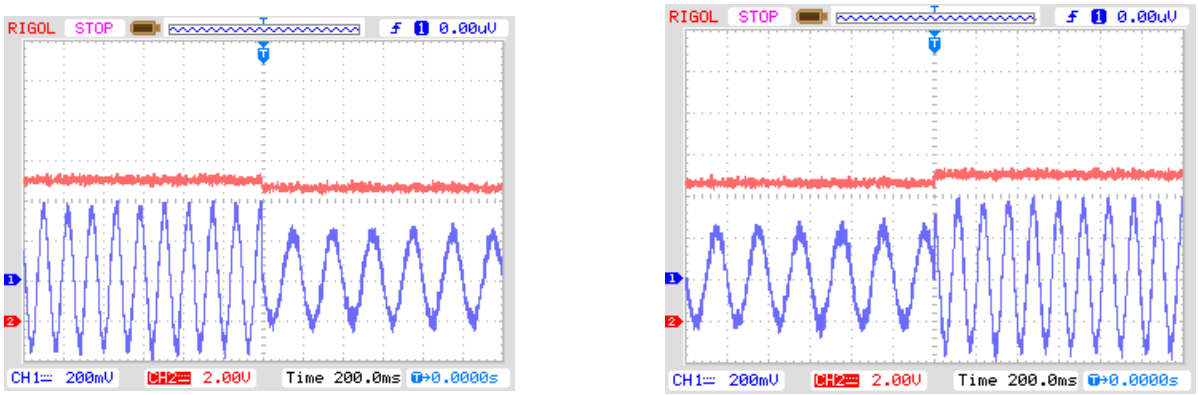

(a) (b)

Fig. 15. Rotor current changes a) with decreasing wind speed, b) with increasing wind speed (CH1: 0.5A/div and CH2: 1000rpm/div).

7. Conclusion

This paper introduced a new topology for DFIG, in which T-type three-level converters are used in back-to-back form instead of conventional converters. It is proved that typical switching approaches including PWM and hysteresis patterns are applicable for T-type converters. The paper also provides a predictive approach based on the DFIG model to control rotor current. A new equation has been extracted to calculate rotor current reference which can be used for both synchronization of DFIG and after grid connection. In addition to simulating the suggested topology, it has also been practically tested in a laboratory setup. The results indicate that the proposed structure can provide appropriate dynamic performance, which can be now used as substitute for conventional structure. Simplicity of the T-type converter implementation in practice is another property of the suggested topology, which enables its control and implementation more encouraged than any other structures.

Future work ought to focus on other aspects of the proposed structure like as detail comparison with similar structures such as 2-level based topologies and detailed consideration of the efficiency and switching losses. In addition, more exhaustive tests on the constructed T-type based topology is highly desirable in the future works to establish more reliable structure for DFIG wind energy conversion applications.

References

[1] G. Abad, J. López, M. Rodríguez, L. Marroyo, and G. Iwanski, Doubly Fed Induction Machine: Modeling and Control for Wind Energy Generation Applications: Wiley-IEEE Press, 2011.

[2] S. Kouro, M. Malinowski, K. Gopakumar, J. Pou, L. G. Franquelo, W. Bin, et al., "Recent Advances and Industrial Applications of Multilevel Converters," Industrial Electronics, IEEE Transactions on, vol. 57, pp. 2553-2580, 2010.

[3] F. Blaabjerg, M. Liserre, and M. Ke, "Power Electronics Converters for Wind Turbine Systems," Industry Applications, IEEE Transactions on, vol. 48, pp. 708-719, 2012.

[4] J. M. Carrasco, L. G. Franquelo, J. T. Bialasiewicz, E. Galvan, R. C. P. Guisado, M. A. M. Prats, et al., "Power-Electronic Systems for the Grid Integration of Renewable Energy Sources: A Survey," Industrial Electronics, IEEE Transactions on, vol. 53, pp. 1002-1016, 2006.

[5] W. Gang, C. Yu, Z. Pengcheng, and K. Yong, "Nine-Switch-Converter-based DFIG Wind Power System and its dynamic port-current assigned approach for Low Voltage Riding Through (LVRT)," in Applied Power Electronics Conference and Exposition (APEC), 2015 IEEE, 2015, pp. 1324-1330.

[6] Pe, x00F, R. a, R. Cardenas, E. Reyes, J. Clare, et al., "A Topology for Multiple Generation System With Doubly Fed Induction Machines and Indirect Matrix Converter," Industrial Electronics, IEEE Transactions on, vol. 56, pp. 4181-4193, 2009.

[7] L. Ting, Z. Zhengming, Z. Yingchao, and Y. Liqiang, "Design of energy storage component parameters for three-level grid-connected inverter," in Electrical Machines and Systems (ICEMS), 2011 International Conference on, 2011, pp. 1-5.

[8] K. Fujii, T. Kikuchi, H. Koubayashi, and K. Yoda, "1-MW advanced T-type NPC converters for solar power generation system," in Power Electronics and Applications (EPE), 2013 15th European Conference on, 2013, pp. 1-10.

[9] M. Schweizer and J. W. Kolar, "Design and Implementation of a Highly Efficient Three-Level T-Type Converter for Low-Voltage Applications," Power Electronics, IEEE Transactions on, vol. 28, pp. 899-907, 2013.

[10] R. Ajabi-Farshbaf and M. R. Azizian, "Slip power recovery of induction machines using three-level T-Type converters," in Power Electronics, Drive Systems and Technologies Conference (PEDSTC), 2014 5th, 2014, pp. 483-487.

[11] P. Alemi, J. Yoon-Cheul, and L. Dong-Choon, "DC-Link Capacitance Minimization in T-Type Three-Level AC/DC/AC PWM Converters," Industrial Electronics, IEEE Transactions on, vol. 62, pp. 1382-1391, 2015.

[12] J. L. Elizondo, A. Olloqui, M. Rivera, M. E. Macias, O. Probst, O. M. Micheloud, et al., "Model-Based Predictive Rotor Current Control for Grid Synchronization of a DFIG Driven by an Indirect Matrix Converter," Emerging and Selected Topics in Power Electronics, IEEE Journal of, vol. 2, pp. 715-726, 2014.

[13] J. Hu, J. Zhu, and D. Dorrell, "Predictive Direct Power Control of Doubly Fed Induction Generators under Unbalanced Grid Voltage Conditions for Power Quality Improvement," Sustainable Energy, IEEE Transactions on, vol. PP, pp. 1-8, 2015.

[14] L. Xiangjie and K. Xiaobing, "Nonlinear Model Predictive Control for DFIG-Based Wind Power Generation," Automation Science and Engineering, IEEE Transactions on, vol. 11, pp. 1046-1055, 2014.

[15] S. A. Davari, "Predictive rotor control of DFIG supplied with back-back converters for variable speed wind turbine application," in Industrial Electronics (ISIE), 2014 IEEE 23rd International Symposium on, 2014, pp. 1415-1419.

[16] J. Rodriguez and P. Cortes, Predictive Control of Power Converters and Electrical Drives, First ed. U.K.: John Wiley & Sons, Ltd., 2012.

[17] P. Cortes, M. P. Kazmierkowski, R. M. Kennel, D. E. Quevedo, and J. Rodriguez, "Predictive Control in Power Electronics and Drives," Industrial Electronics, IEEE Transactions on, vol. 55, pp. 4312-4324, 2008.

[18] S. Chikha, K. Barra, and A. Reama, "Predictive current control of a wind energy conversion system based DFIG via direct matrix converter," in Renewable Energy Congress (IREC), 2015 6th International, 2015, pp. 1-7.

[19] J. Sayritupac, E. Albanez, J. Rengifo, J. M. Aller, and J. Restrepo, "Predictive control strategy for DFIG wind turbines with maximum power point tracking using multilevel converters," in Power Electronics and Power Quality Applications (PEPQA), 2015 IEEE Workshop on, 2015, pp. 1-6.

[20] Y. Xibo, "Analytical averaged loss model of a three-level T-type converter," in Power Electronics, Machines and Drives (PEMD 2014), 7th IET International Conference on, 2014, pp. 1-6.

[21] A. Mokhberdoran and A. Ajami, "Symmetric and Asymmetric Design and Implementation of New Cascaded Multilevel Inverter Topology," Power Electronics, IEEE Transactions on, vol. 29, pp. 6712-6724, 2014.

Appendices

Appendix 1

Constants λ_1 to λ_{18} are shown in terms of machine parameters, as follow:

$\lambda_1=(\frac{1}{L_sL_r-L_m^2})$ $\lambda_2=L_r$ $\lambda_3=-L_m$

$\lambda_4=L_s$ $\lambda_5=R_sL_r$ $\lambda_6=\omega_sL_sL_r$

$\lambda_7=L_m^2$ $\lambda_8=L_s^2$ $\lambda_9=L_mR_r$

$\lambda_{10}=\omega_sL_mL_r$ $\lambda_{11}=L_sL_m$ $\lambda_{12}=R_sL_r$

$\lambda_{13}=L_mL_r$ $\lambda_{14}=R_sL_m$ $\lambda_{15}=\omega_sL_sL_m$

$\lambda_{16}=R_rL_s$ $\lambda_{17}=\omega_sL_m^2$ $\lambda_{18}=L_sL_r$

Appendix 2

Machine parameters which is used in simulations

Nominal Power	1.5 MW
Nominal Voltage	575 V

Frequency	50 Hz
R_s	0.023 pu
L_{is}	0.18 p.u
R_r	0.016 pu
L_{ir}	0.16 pu
L_m	2.9 pu
Pairs of poles	3
Moment of inertia	0.685 Kg.m^2

Parameters of the DFIG, used for practical results

Nominal Power	0.25 kW
Nominal Voltage	120 V
Frequency	50 Hz
R_s	1.7 Ω
L_{is}	0.012 H
R_r	1.6 Ω
L_{ir}	0.012 H
L_m	0.379 H
Pairs of poles	1
Moment of inertia	0.03 Kg.m^2